JJC Jordan Journal of Chemistry Vol. 10 No.3, 2015, pp. 161-178

Theoretical Study of 3-Amino-1,2,4-Triazole and Its Protonated Analogue as Corrosion Inhibitors

Fahimeh Shojaie*

Department of Photonic, Institute of Science and High Technology and Environmental Sciences, Graduate University of Advanced Technology, Kerman, Iran

Received on June 14, 2015 **Accepted on** July 30, 2015

Abstract

Quantum chemical calculations were performed on 3-Amino-1,2,4-Triazole (ATA) which may be used as a corrosion inhibitor for austenitic stainless steel. The quantum chemical properties of ATA that are most relevant to its potential action as a corrosion inhibitor have been calculated in the gas phase and in solution for comparison purposes. Calculations were carried out to study the adsorption of the protonated forms of ATA on metal surfaces. The molecular properties of the protonated ATA species were compared to those of neutral ATA to determine the preferred species that bind to the metal surface.

Keywords: Protonated forms; 3-Amino-1,2,4-Triazole (ATA); Corrosion; Density Functional Theory (DFT).

Introduction

Quantum chemical methods are useful for determining the molecular structure of chemical compounds. These methods also elucidate the electronic structure and reactivity.[1,2] Therefore, quantum chemical calculations can be used to analyze the molecular electronic structure of corrosion inhibitors and corrosion inhibition mechanisms. The density functional theory DFT has been widely used to predict the geometric and electronic properties of compounds with a potential application in corrosion inhibition and also to study the binding properties of compounds on metal surfaces.[3-6] DFT/B3LYP has been widely used to study the chemical reactivity and selectivity of molecules as well as the mechanisms of inhibitors binding to metal surfaces.[7, 8]

Heterocyclic organic compounds are frequently responsible for good corrosion inhibition due to adsorption onto the surface.[9,10] Several studies have been performed that show the potential role of triazole and benzotriazole derivatives as corrosion inhibitors.[11-13] These studies were done in different environments and by theoretical quantum chemical calculation methods.[14-17] In Addition, theoretical studies on 3-Amino-1,2,4-Triazole (ATA), BTAH (benzotriazole), and BTAOH (1-hydroxybenzotri-

* Corresponding author: e-mail: f.shojaie@kgut.ac.ir

azole) as inhibitor molecules on Cu (111) surface show that the strength of the chemisorption of ATA is more than that of BTAH and BTAOH.[18] Awad et al. performed molecular orbital calculations on four triazole derivatives in order to simulate the adsorption mode of the inhibitor on the metal surface.[19] Magdy et al. studied the corrosion inhibition effect of ATA in 2.5 M NaCl solution. They showed that ATA was a good inhibitor for several materials whose corrosion properties were investigated in 2.5 M NaCl solutions.[20] The effect of sulphur atom in thiazole derivatives as corrosion inhibitors have also been studied.[21] The objective of this paper is to carry out a theoretical study on ATA and its protonated analogue as corrosion inhibitors.

Results and Discussion

Computational methodology

Theoretical calculations were carried out for the title compounds using the Gaussian 09 program.[22] Theoretical calculations were carried out using B3LYP/6-31G++ (d, p) to obtain more reliable energies for all the stationary points on the potential energy surface (PES). The G3 method[23] was used to calculate the single point energies at the B3LYP/6-311++G (d, p) optimized geometries. It is anticipated that the properties of molecules and ions are different in the gas phase and in solution. In this work, all calculations for the solvent effect in water were carried out using the integral equation formalism of the polarized continuum model (IEFPCM).[24] It seems that this method is more suitable for our purpose, because it has been found to be very useful and can describe accurately the charge distribution of solute outside of the PCM cavity.[25-27] The IEFPCM method exploits a single common approach for dielectrics of very different nature and it allows reaching a unified analytical solution of the electrostatic interaction for all solute–solvent systems.[28] The reactive ability of the ATA inhibitor is closely linked to its highest occupied molecular orbital (HOMO), lowest unoccupied molecular orbital (LUMO) and energy gap (ΔE), as well as other parameters such as the global hardness (η), global softness (σ), dipole moment (μ), the fraction of electron transferred (ΔN)… etc.[29] The ATA local reactivity has been analyzed by means of the Fukui indices. These indices indicate the reactive regions in the form of the nucleophilic and electrophilic behaviour of each atom in the molecule.[30]

Reactivity parameters

The structure and the optimized configuration of ATA are shown in Figure 1. The inhibitor conformer is considered to be minima based on the absence of imaginary frequencies. Figure 1 shows the optimized geometry of all stationary points at the B3LYP/6-311++G (d, p) level of theory for both gas and liquid phases. A comparison between bond lengths and angles for gas phase and those for liquid phase shows the effect of solvent on the geometry. Figure 1 shows that bond lengths and angles involving nitrogen atoms are slightly affected in the solution state than in the gas phase.

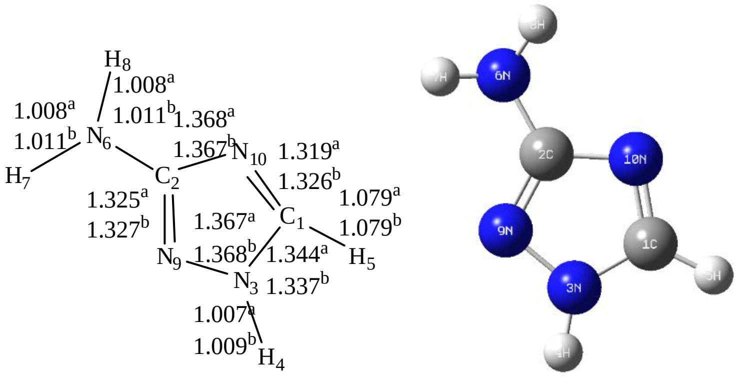

D(C1,N10,C2)= 102.847[a], 102.957[b]. D(N6,C2,N9)= 123.137[a], 123.162[b].
D(C1,N3,N9)= 110.244[a], 110.318[b].

Figure 1: Structure and optimized geometry of ATA (using B3LYP/6-31++G (d, p)). Bond lengths are in angstroms and angles are in degrees: [a] gas phase and [b] liquid phase.

The HOMO and the LUMO of the studied inhibitor are shown in Figure 2. In the ATA molecule, the HOMO is delocalized on atom N3 and the LUMO is delocalized on C1 and N10. The regions of a molecule on which the HOMO is distributed indicate the sites which have the highest tendency to interact with a metal surface. The LUMO indicates regions which have the highest tendency to accept electrons.

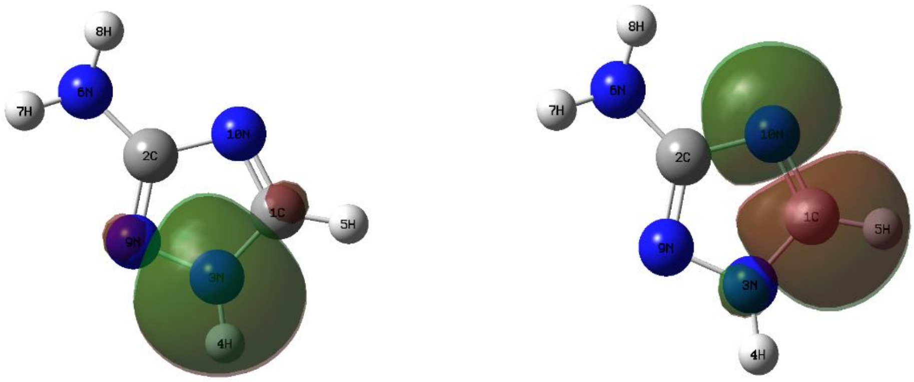

HOMO LUMO

Figure 2: HOMO and LUMO of the non-protonated inhibitor molecule (using B3LYP/6-31++G (d, p)).

Table 1 shows the quantum chemical descriptors of the ATA inhibitor. These descriptors give information about the chemical reactivity of the ATA molecule in the gas phase and in solution. These descriptors were calculated by B3LYP and G3 methods using both Energetic and Orbital modes. In order to obtain more reliable energies of all stationary points on the PES, the G3 method was used to calculate the single point energies at the B3LYP/6-311++G (d, p) optimized geometries. The PES energies were also calculated using G3 (a) and MP2 (b) methods.

Table1: Quantum chemical descriptors for the studied compound: ^{a} MP2 and ^{b} G3.

Molecular descriptors	Parameter	B3LYP		G3	
		Gas	Solvent	Gas	Solvent
HOMO (eV)	-	-6.250	-6.486	-9.136	-9.385
LUMO (eV)	-	-0.376	-0.238	0.926	1.220
ΔE (eV)	-	5.875	6.248	10.062	10.604
Ionization Potential (IP) IP=[E(+1)-E(0)]	Energetic	8.607	6.507	8.368^{a}, 8.661^{b}	6.200^{a},6.505^{b}
IP=$-E_{HOMO}$	Orbital	6.250	6.486	9.136	9.385
Electron Affinity(EA)(eV) EA=[E(0)-E(-1)]	Energetic	-0.474	0.867	-1.297^{a},-1.773^{b}	1.028^{a},0.576^{b}
EA=$-E_{LUMO}$	Orbital	0.376	0.238	-0.926	-1.220
Global hardness(η) (eV)	Energetic	4.541	2.820	4.833^{a},5.217^{b}	2.586^{a},2.965^{b}
η=(I-A)/2	Orbital	2.937	3.124	5.031	5.302
Chemical potential (χ) (eV) χ=(I+A)/2	Energetic	4.067	3.687	3.536^{a},3.444^{b}	3.614^{a},3.541^{b}
	Orbital	3.313	3.362	4.105	4.083
Global softness(σ) (eV^{-1})	Energetic	0.220	0.355	0.207^{a},0.192^{b}	0.387^{a},0.337^{b}
σ=1/η	Orbital	0.340	0.320	0.199	0.189
Electrophilicity(ω) (eV)	Energetic	1.821	2.411	1.293^{a},1.137^{b}	2.525^{a},2.114^{b}
$\omega=\chi^2/2\eta$	Orbital	1.868	1.809	1.675	1.572
Electrodonating (ω^-) (eV)	Energetic	4.422	4.607	3.665^{a},3.511^{b}	4.656^{a},4.255^{b}
$\omega^-=(3I+A)^2/16(I-A)$	Orbital	3.892	3.881	4.356	4.276
Electroaccepting (ω^+) (eV) $\omega^+=(I+3A)^2/16(I-A)$	Energetic	0.355	0.920	0.130^{a},0.067^{b}	1.042^{a},0.714^{b}
	Orbital	0.579	0.519	0.251	0.193
net electrophilicity ($\Delta\omega^{\pm}$) (eV) $\Delta\omega^{\pm}=\omega^{+}+\omega^{-}$	Energetic	4.777	5.526	3.795^{a},3.577^{b}	5.697^{a},4.969^{b}
	Orbital	4.471	4.400	4.607	4.469
Transferred electrons(ΔN) $\Delta N=(\chi_{Fe}-\chi_{inh})/2(\eta_{Fe}+\eta_{inh})$	Energetic	0.323	0.587	0.358^{a},0.341^{b}	0.655^{a},0.583^{b}
	Orbital	0.628	0.582	0.288	0.275
Total Negative Charge (TNC)	-	-2.097	-2.173	-2.348	-2.535
Dipole moment (μ) (D)	-	2.029	2.869	2.469	3.325
ET (a.u)	-	-297.703	-297.717	-297.425^{a},-297.327^{b}	-297.438^{a},-297.339^{b}

The Ionization Potential (IP) is a basic descriptor of the chemical reactivity of atoms and molecules. A lower IP indicates less difficulty to remove electrons from a system.[33] Table 1 shows that ATA has a lower IP in the liquid phase than in the gas phase if calculated by the B3LYP method using the energy mode and has a lower IP in the gas phase than in the liquid phase if calculated by same method using the orbital mode.

The direction of charge transfer is determined by the chemical potential of a molecule. An electrophile is a chemical species capable of accepting electrons from its environment. The energy of an electrophile must decrease upon accepting electronic charge. The chemical potential of ATA is negative. This means that when ATA is in contact with a metal, electrons are transferred from ATA to the metal surface.

Absolute global hardness (η) and global softness (σ) are important properties for measuring the molecular stability and reactivity. It could be seen from their calculated values in Table 1 that ATA has, according to the orbital parameter method, lower η and higher σ values in the gas phase, which indicates the high reactivity of this molecule in the gas phase. The energy difference between the HOMO and LUMO (ΔE) is a measure of the molecule softness. A hard molecule has a large ΔE and a soft molecule has a small ΔE.[34] Soft molecules are more reactive than hard ones because they could easily transfer electrons to an acceptor. ATA is a soft molecule in the gas phase because it has a smaller ΔE in this phase than in the liquid phase. This shows the relationship between molecular softness and energy gap (by the orbital parameter method) in ATA.

The ability of a molecule to accept electrons is described by the electrophilicity index. Electrophilicity is a measure of the energy stabilization after a system accepts the additional amount of electron charge from its environment.[35] In our study, we have calculated a low value of electrophilicity for ATA in the gas phase. Therefore, ATA is a strong nucleophile in the gas phase and a weak nucleophile in the liquid phase.

Based on calculations using the energetic mode, Table 1 shows that ATA is a better electron donor in the gas phase, but orbital mode calculations indicates that ATA is a better electron donor in the liquid phase. A small electrodonating value makes a system to be a better electron donor.[36] Energetic mode calculations indicate that ATA has a better capability of accepting charge in the liquid phase, whereas orbital mode calculations indicate that the molecule has the same capability in the gas phase as in the liquid phase. Energetic mode calculations give a total electrophilicity that shows ATA to be a strong nucleophile in the gas phase.

The electron donation of an inhibitor is described by ΔN.[37] If ΔN is below 3.6 eV, then the inhibition efficiency increases with increasing the electrodonating ($\omega -$) ability at a mild steel interface.[38] All values of ΔN in Table 1 are below 3.6 eV. Orbital mode calculations indicate that for ATA ΔN is higher in the gas phase, whereas energetic mode calculations show ATA to have higher ΔN in the liquid phase. Because iron is the major constituent of austenitic stainless steel, the theoretical values of the iron electronegativity (χ_{Fe}=7 eV) and the iron global hardness (η_{Fe}=0) are used to compute ΔN for the various Hamiltonians.[39]

The calculations show that ATA has the highest values of the Total Negative Charge (TNC) in gas and solution states. This property indicates that the adsorption of the inhibitor onto a mild steel surface is enhanced at higher TNC values. The TNC values of the ATA molecule are higher in the liquid phase than in the gas phase.

Information about the polarity of the molecule is given by the dipole moment μ. A high value of μ corresponds probably to enhanced adsorption of the chemical compound onto a metal surface.[40] It is clear from Table 1 that μ is higher in water than in the gas phase and this is an indication of the polarization effect of the solvent on the ATA inhibitor molecule. The difference between the ATA dipole moment in the gas phase and that in water was calculated by the B3LYP method to be 0.840 Debye whereas the G3 method calculates this difference to be 0.859 Debye.

The stabilization effect of solvent causes a significant decrease in the Total Energy (ET) values of the ATA inhibitor. The ET values show that ATA is more stable in the liquid phase than in the gas phase.

Local molecular reactivity

Selectivity parameters reveal the regions of a molecule that are likely to interact with a metal surface. These parameters include the atomic charges, distribution of frontier molecular orbital and the Fukui functions. The atom with the highest negative partial atomic charge interacts most strongly with a metal surface through a donor-acceptor type of interaction because it represents the site with the highest electron density.[41,42] The Mulliken atomic charges and the natural bond orbital (NBO) of the atoms of the studied compound in the gas phase as well as in solution calculated both by B3LYP and G3 methods are reported in Table 2. For ATA, the highest negative charge is on the N3, N6, N9 and N10 atoms and that in both phases, the charges on these atoms being however higher in the liquid phase. Because nitrogen atoms have a lone pair of electrons, these could be donated to the vacant *s* or partially filled *d* orbitals of the metal and thereby facilitate the adsorption of the ATA inhibitor on a metal surface.

Table2: Calculated Mulliken atomic charges for ATA using the B3LYP/++6-31G (d,p) and G3 methods.

atom	**B3LYP Gas**		**G3 Gas**		**B3LYP Solvent**		**G3 Solvent**	
	Mulliken	NBO	Mulliken	NBO	Mulliken	NBO	Mulliken	NBO
C1	0.019	0.216	0.211	0.352	0.031	0.229	0.239	0.369
C2	-0.047	0.504	0.392	0.640	-0.007	0.506	0.432	0.644
N3	-0.213	-0.365	-0.189	-0.416	-0.199	-0.353	-0.182	-0.409
H4	0.321	0.407	0.229	0.411	0.364	0.43	0.266	0.435
H5	0.169	0.198	0.189	0.188	0.216	0.217	0.229	0.209
N6	-0.326	-0.803	-0.401	-0.841	-0.378	-0.818	-0.451	-0.959
H7	0.253	0.386	0.210	0.380	0.277	0.395	0.234	0.39
H8	0.254	0.387	0.203	0.379	0.277	0.395	0.226	0.389
N9	-0.172	-0.382	-0.308	-0.444	-0.241	-0.412	-0.377	-0.476
N10	-0.259	-0.547	-0.536	-0.648	-0.34	-0.59	-0.616	-0.691

The Fukui indices f^+ and f^- permit the distinction between reactive and non-reactive regions of a system. They determine the nucleophilic and electrophilic behaviour of a molecule as well as its chemical reactivity. The maximum of f^+ corresponds to reactivity with respect to a nucleophilic attack and the maximum of f^- shows the preferred site for adsorption of electrophilic agents. These functions can be given by Equations (1) and (2):[16]

$$f^+ = Q_{N+1} - Q_N \qquad \text{Equation (1)}$$

$$f^+ = Q_N - Q_{N-1} \qquad \text{Equation (2)}$$

Q_{N+1} is an anion with an electron added to the LUMO of its neutral molecule while Q_{N-1} is a cation with an electron removed from the HOMO of its neutral molecule. Thus, Q_{N+1}, Q_N and Q_{N-1} are anionic, neutral and cationic states, respectively. For ATA, the highest f^+ and f^- are associated with the N6 atom and that both in the gas phase and in solution. The calculated values of the Fukui functions are reported in Table 3. The binding capability of a metal to an inhibitor depends strongly on the electronic charge of the inhibitor active site. In a corrosion system, the inhibitor acts as a Lewis base (nucleophilic) while the metal acts as a Lewis acid (electrophilic). In both phases, the Mulliken atomic charges and the Fukui indices of the non-protonated ATA species show that the N6 atom has the highest negative charge and the highest f^-, respectively. Thus, the ATA inhibitor molecule is expected to interact with the Fe metal through the N6 atom.

The following conclusions may be drawn using the molecular properties of the ATA neutral species:

(1) The quantum chemical descriptors of ATA obtained for the gas phase and the solution states using the energetic mode are different from those obtained using the orbital mode.

(2) The effect of solvation (using water as a solvent) on the ATA corrosion inhibition efficiency is important.

(3) The effect of solvation (using water as solvent) on the quantum chemical descriptors data calculated using the energetic mode is larger than in the case of orbital mode calculations. For example, the difference between the Transferred Electrons charges in the gas phase and in water calculated by the B3LYP method using the energetic mode was 0.264 whereas the same method using the orbital mode gives a value of -0.046 for this difference.

(4) The results of LUMO and HOMO calculations (Figure 2) are different from the results of the Mulliken atomic charges and Fukui functions (Table3).

(5) The N6 atom has the highest negative charge both in the gas phase as well as in solution (except Mulliken charges using the G3 method).

Calculations for the protonated ATA species

The protonation of the ATA inhibitor at nitrogen atoms with a number of lone pairs of electrons is caused by the interaction between the acidic medium and the inhibitor. In such cases, the characteristics of the ATA corrosion inhibitor in the protonated and non-protonated forms could determine the preferred form of the inhibitor that can interact with a metal surface. All possibilities for protonation at the active sites were considered. The four atoms on which ATA could be protonated are N3, N6, N9 and N10.

Table3: Calculated Fukui functions for ATA using B3LYP/++6-31G (d, p) and G3 methods.

atom	B3LYP								G3							
	Gas				Solvent				Gas				Solvent			
	Q_{N+1}	Q_{N-1}	$\lvert f^{+}\rvert$	$\lvert f^{-}\rvert$	Q_{N+1}	Q_{N-1}	$\lvert f^{+}\rvert$	$\lvert f^{-}\rvert$	Q_{N+1}	Q_{N-1}	$\lvert f^{+}\rvert$	$\lvert f^{-}\rvert$	Q_{N+1}	Q_{N-1}	$\lvert f^{+}\rvert$	$\lvert f^{-}\rvert$
C1	0.116	0.171	0.100	0.045	0.114	0.179	0.115	0.050	0.456	0.251	0.620	0.101	0.448	0.253	0.079	0.116
C2	0.252	0.286	0.252	0.218	0.258	0.288	0.248	0.218	0.303	0.287	0.464	0.352	0.308	0.268	0.336	0.376
N3	-0.176	-0.067	0.189	0.298	-0.177	-0.062	0.176	0.291	-0.268	-0.152	0.457	0.264	-0.269	-0.149	0.140	0.260
H4	0.213	0.224	0.194	0.183	0.214	0.230	0.216	0.200	0.176	0.223	0.843	0.188	0.187	0.228	0.248	0.207
H5	0.102	0.125	0.096	0.073	0.107	0.126	0.110	0.091	0.041	0.117	0.013	0.070	0.055	0.119	0.154	0.090
N6	-0.405	-0.022	0.398	0.781	-0.420	-0.020	0.398	0.798	-0.432	-0.101	1.014	0.740	-0.438	-0.076	0.521	0.883
H7	0.191	0.210	0.195	0.176	0.207	0.213	0.188	0.182	0.175	0.213	0.619	0.166	0.185	0.216	0.205	0.174
H8	0.191	0.213	0.196	0.174	0.201	0.215	0.194	0.180	0.173	0.214	0.763	0.164	0.185	0.215	0.204	0.174
N9	-0.196	0.080	0.186	0.462	-0.208	0.070	0.204	0.482	-0.239	0.236	0.444	0.680	-0.259	0.230	0.217	0.706
N10	-0.287	-0.219	0.260	0.328	-0.296	-0.240	0.294	0.350	-0.385	-0.289	0.648	0.359	-0.401	-0.304	0.290	0.387

The structure and the optimized configuration of the protonated species are shown in Figure 3. The structures of these species are considered to be minima based on the absence of imaginary frequencies. Figure 3 shows also the optimized geometry of all stationary points at the B3LYP/6-311++G (d, p) level of theory in both gas phase and in solution.

protonated molecules	structures	angles	optimized geometries
Protonation at N3	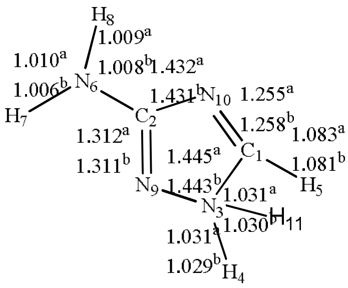	D(C1,N10,C2)= 105.967[a], 105.415[b]. D(N6,C2,N9)= 125.979[a], 126.039[b]. D(C1,N3,N9)= 105.513[a], 105.563[b].	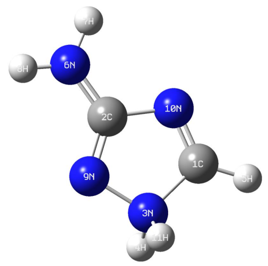
Protonation at N6	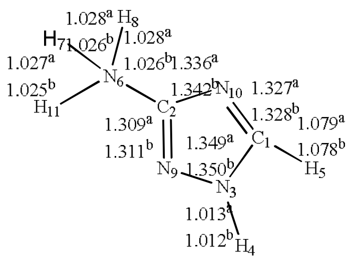	D(C1,N10,C2)= 101.289[a], 101.611[b]. D(N6,C2,N9)= 119.992[a], 120.420[b]. D(C1,N3,N9)= 110.679[a], 110.591[b].	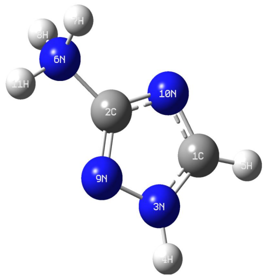
Protonation at N9	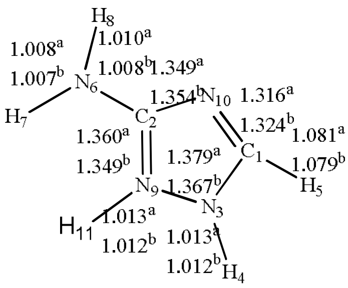	D(C1,N10,C2)= 105.392[a], 105.130[b]. D(N6,C2,N9)= 125.395[a], 125.133[b]. D(C1,N3,N9)= 105.945[a], 106.438[b].	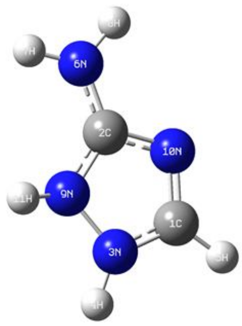
Protonation at N10	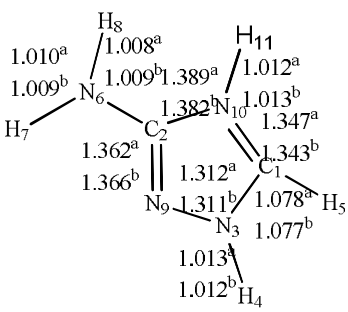	D(C1,N10,C2)= 107.128[a], 107.255[b]. D(N6,C2,N9)= 125.828[a], 125.836[b]. D(C1,N3,N9)= 113.270[a], 112.902[b].	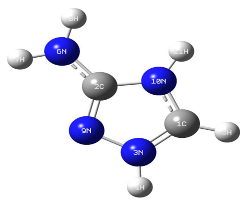

Figure 3: The structures and the optimized geometries of the inhibitor under study. Bond lengths are in angstroms and bond angles are in degrees. [a] gas phase and [b] liquid phase.

A comparison of the bond length and bond angle values obtained in the gas phase and those obtained in solution shows the effect of solvent on the geometry. The bond lengths and bond angles involving nitrogen atoms are more affected by protonation in the liquid phase than in the gas phase. The HOMO and the LUMO of the studied inhibitor, both in the gas phase and in solution, are shown in Figure 4. The HOMO of the N3-protonated ATA molecule is delocalized on the N6 atom and its LUMO is delocalized on the C1 atom. This implies that the N6 site of the N3-protonated ATA molecule has the highest tendency to interact with a metal surface. The HOMO and the LUMO of an N6-protonated ATA are delocalized on the N3 and N9 atoms, respectively. This means that the N9 site has the highest tendency to interact with a metal surface. The N3 site has the highest tendency to accept electrons because the HOMO is delocalized on N3 and N9 atoms and LUMO is delocalized throughout the system except on N3 and C1 atoms. The HOMO of an N10-protonated ATA molecule is delocalized on the N6 atom and its LUMO is delocalized on the C1 and N3 atoms. This means that the N6 site has the highest tendency to interact with a metal surface.

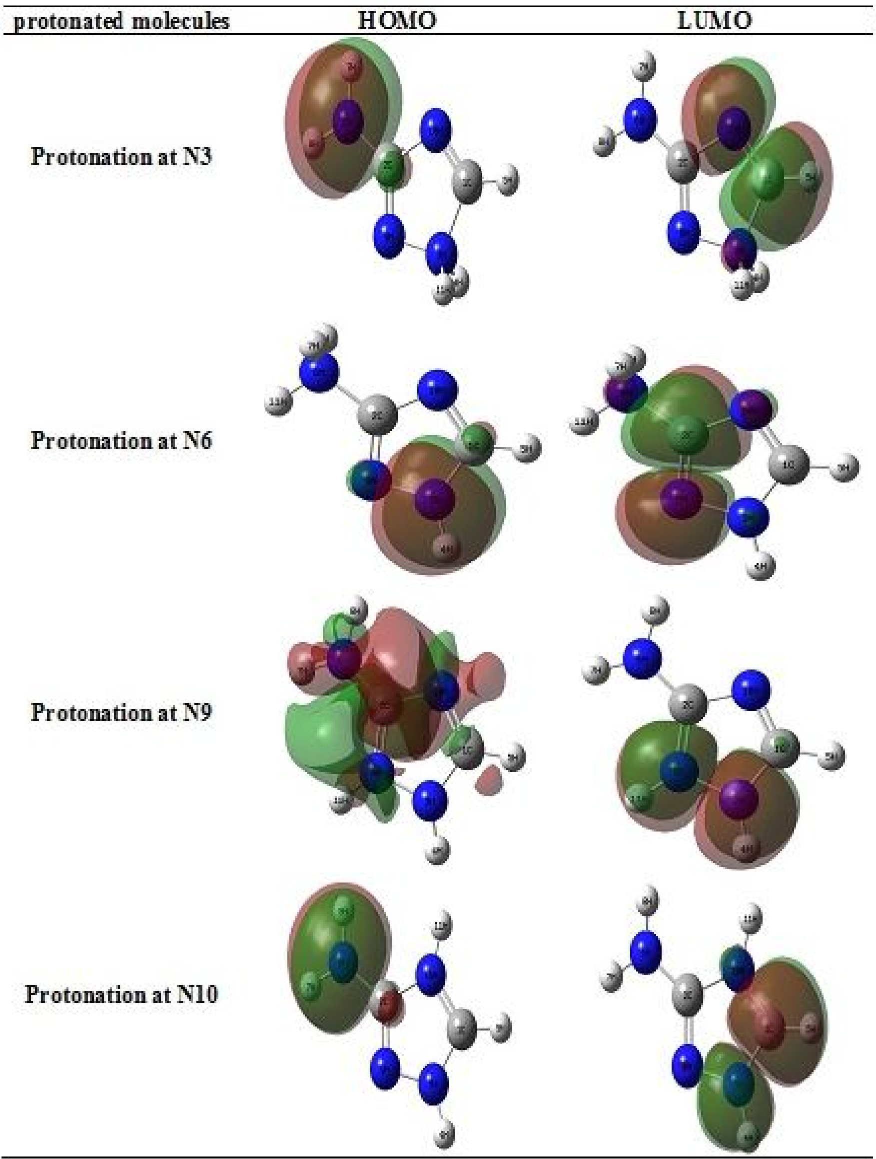

Figure 4: HOMO and LUMO of the protonated molecules (using B3LYP/6-31++G (d,p)).

Table 4 shows the quantum chemical descriptors of the protonated ATA compounds. B3LYP calculations indicate that the protonated forms of the ATA have lowest ΔE and LUMO energies in the gas phase. This means that the ATA molecule acts as a better corrosion inhibitor in the gas phase than in the liquid phase. It can be seen in Table 4 from the data obtained by the B3LYP method that protonation at the N10 site gives the highest HOMO, both in the gas phase and in solution. The B3LYP data for protonation at the N3 site give the lowest energy gap for the two phases, whereas the G3 data gives for same protonation the lowest energy gap for the gas phase.

Based on the G3 data, the protonated forms have the lowest η and the highest σ values in the liquid phase, which indicates the high reactivity of this molecule in the liquid phase. In contrast to the data of the G3 method, the B3LYP data show lowest η and highest σ values for the gas phase, which indicates the high reactivity of these molecules in the gas phase. The B3LYP data of protonation at the N6 site have highest η values for the two phases.

The dipole moment μ is higher in the liquid phase than in the gas phase, which is the effect of the polarization of the protonated ATA species by the solvent resulting in an increased charge separation in the solute. The G3 data for protonation at the N10 site gives the highest μ for the two phases. The TNC of the protonated forms calculated by both B3LYP and G3 methods is higher in aqueous solution than in the gas phase. The TNC calculated by the G3 method for protonation at the N10 site is higher for the two phases than the TNC data of the G3 method for protonation at the N3, N6 and N9 sites.

The Mulliken atomic charges and NBO of the atoms of protonated ATA in the gas phase and in solution are reported in Tables 5 and 6. Both B3LYP and G3 methods give the highest negative charge on N3, N6, N9 and N10 atoms in both phases and the highest charges on these atoms in the liquid phase. Because nitrogen atoms have a lone pair of electrons, these lone pairs of electrons could be donated to the vacant *s* or partially filled *d* orbitals of the metal and thereby facilitate the adsorption of the ATA inhibitor on a metal surface.

Table4: Quantum chemical descriptors for the protonated compounds.

Molecular descriptors	B3LYP Protonation at N3		B3LYP Protonation at N6		B3LYP Protonation at N9		B3LYP Protonation at N10		G3 Protonation at N3		G3 Protonation at N6		G3 Protonation at N9		G3 Protonation at N10	
	Gas	Solvent	Gas	Solvent	Gas	Solvent	Gas	Solvent	Gas	Solvent	Gas	Solvent	Gas	Solvent	Gas	Solvent
HOMO (eV)	-12.390	-8.119	-12.893	-11.832	-12.324	-7.828	-11.832	-7.590	-15.680	-11.449	-15.303	-11.162	-15.421	-11.082	-14.708	-10.561
LUMO (eV)	-7.334	-2.845	-5.468	-1.113	-6.213	-1.596	-6.188	-1.655	-3.064	1.073	-3.046	1.030	-2.670	1.085	-2.642	1.075
ΔE (eV)	5.056	5.274	7.426	10.720	6.111	6.232	5.644	5.935	12.616	12.523	12.257	12.192	12.751	12.167	12.065	11.636
$I=-E_{HOMO}$	12.390	8.119	12.893	11.832	12.324	7.828	11.832	7.590	15.680	11.449	15.303	11.162	15.421	11.082	14.708	10.561
$A=-E_{LUMO}$	7.334	2.845	5.468	1.113	6.213	1.596	6.188	1.655	3.064	-1.073	3.046	-1.030	2.670	-1.085	2.642	-1.075
$\eta=(I-A)/2$	2.528	2.637	3.713	5.360	3.056	3.116	2.822	2.967	6.308	6.261	6.128	6.096	6.376	6.084	6.033	5.818
$\chi=(I+A)/2$	9.862	5.482	9.180	6.473	9.269	4.712	9.010	4.622	9.372	5.188	9.175	5.066	9.045	4.999	8.675	4.743
$\sigma=1/\eta$	0.396	0.379	0.269	0.187	0.327	0.321	0.354	0.337	0.159	0.160	0.163	0.164	0.157	0.164	0.166	0.172
$\omega=\chi^2/2\eta$	19.235	5.698	11.350	3.908	14.057	3.562	14.384	3.600	6.962	2.149	6.868	2.105	6.416	2.053	6.238	1.933
$\omega^-=(3I+A)^2/16(I-A)$	24.482	8.769	16.404	7.815	19.074	6.308	19.242	6.282	12.436	5.526	12.221	5.400	11.736	5.313	11.329	5.032
$\omega^+=(I+3A)^2/16(I-A)$	14.620	3.287	7.224	1.342	9.805	1.596	10.232	1.660	3.064	0.338	3.046	0.334	2.691	0.315	2.654	0.289
$\Delta\omega^{\pm}=\omega^+ + \omega^-$	39.103	12.055	23.628	9.157	28.879	7.904	29.474	7.942	15.500	5.864	15.267	5.735	14.427	5.628	13.983	5.32
$\Delta E_T= -\eta/4$	-0.632	-0.659	-0.928	-1.340	-0.764	-0.779	-0.706	-0.742	-1.577	-1.565	-1.532	-1.524	-1.594	-1.521	-1.508	-1.454
$N=(\chi_{Fe}-\Delta\chi_{inh})/2(\eta_{Fe}+\eta_{inh})$	-0.566	0.288	-0.294	0.049	-0.371	0.367	-0.356	0.401	-0.188	0.145	-0.177	0.159	-0.160	0.164	-0.139	0.194
Total Negative charge (TNC)	-1.895	-1.975	-1.759	-1.815	-1.935	-1.956	-1.877	-1.932	-2.169	-2.261	-1.965	-2.033	-2.28	-2.288	-2.15	-2.202
Dipole moment (μ) (D)	3.183	4.284	3.968	4.765	3.868	5.442	3.597	4.791	3.569	4.7607	3.974	4.747	3.818	5.501	4.119	5.4712
ET (a.u)	-298.006	-298.104	-298.039	-298.141	-298.055	-298.149	-298.062	-298.156	-297.619	-297.717	-297.664	-297.764	-297.668	-297.763	-297.680	-297.773

Table5: Calculated Mulliken atomic charges for the protonated compounds in the gas phase using B3LYP/++6-31G (d,p) and G3 methods.

	B3LYP Protonation at N3		B3LYP Protonation at N6		B3LYP Protonation at N9		B3LYP Protonation at N10	
	Mulliken	NBO	Mulliken	NBO	Mulliken	NBO	Mulliken	NBO
C1	0.049	0.309	0.028	0.26	0.083	0.319	0.135	0.289
C2	-0.030	0.562	-0.142	0.444	0.073	0.613	0.111	0.572
N3	-0.307	-0.438	-0.192	-0.320	-0.192	-0.348	-0.213	-0.285
H4	0.363	0.455	0.375	0.443	0.365	0.45	0.399	0.453
H5	0.294	0.248	0.239	0.239	0.257	0.246	0.268	0.259
N6	-0.303	-0.71	-0.230	-0.678	-0.330	-0.727	-0.310	-0.761
H7	0.334	0.434	0.375	0.456	0.310	0.423	0.322	0.434
H8	0.336	0.434	0.375	0.456	0.342	0.141	0.284	0.416
N9	-0.044	-0.373	-0.046	-0.275	-0.080	-0.38	-0.070	-0.299
N10	-0.055	-0.374	-0.146	-0.486	-0.173	-0.48	-0.290	-0.532
H11	0.363	0.455	0.362	0.462	0.348	0.443	0.364	0.453
	G3 Protonation at N3		**G3 Protonation at N6**		**G3 Protonation at N9**		**G3 Protonation at N10**	
	Mulliken	NBO	Mulliken	NBO	Mulliken	NBO	Mulliken	NBO
C1	0.100	0.412	0.206	0.376	0.283	0.477	0.316	0.424
C2	0.523	0.743	0.231	0.540	0.528	0.793	0.484	0.713
N3	0.116	-0.449	-0.182	-0.380	-0.183	-0.417	-0.162	-0.337
H4	0.235	0.452	0.269	0.448	0.276	0.457	0.298	0.459
H5	0.255	0.237	0.241	0.228	0.25	0.233	0.264	0.251
N6	-0.414	-0.792	0.073	-0.687	-0.406	-0.805	-0.349	-0.829
H7	0.264	0.436	0.241	0.456	0.236	0.427	0.263	0.429
H8	0.262	0.436	0.241	0.456	0.276	0.442	0.214	0.413
N9	-0.295	-0.464	-0.164	-0.315	-0.058	-0.446	-0.212	-0.368
N10	-0.282	-0.464	-0.444	-0.583	-0.473	-0.612	-0.376	-0.616
H11	0.235	0.452	0.268	0.462	0.27	0.45	0.26	0.46

Table 6: Calculated Mulliken atomic charges for the protonated compounds using B3LYP/++6-31G (d,p) and G3, in liquid phase.

	B3 Protonation at N3		B3 Protonation at N6		B3 Protonation at N9		B3 Protonation at N10	
	Mulliken	NBO	Mulliken	NBO	Mulliken	NBO	Mulliken	NBO
C1	0.071	0.344	0.034	0.253	0.083	0.307	0.146	0.312
C2	-0.003	0.569	-0.121	0.474	0.097	0.607	0.104	0.576
N3	-0.242	-0.43	-0.178	-0.319	-0.067	-0.32	-0.199	-0.289
H4	0.381	0.472	0.389	0.448	0.0407	0.468	0.413	0.459
H5	0.308	0.253	0.242	0.235	0.255	0.244	0.286	0.267
N6	-0.344	-0.724	-0.192	-0.676	-0.383	-0.743	-0.34	-0.774
H7	0.339	0.433	0.388	0.468	0.328	0.431	0.314	0.425
H8	0.339	0.432	0.388	0.468	0.339	0.434	0.3	0.423
N9	-0.118	-0.401	-0.106	-0.3	-0.067	-0.356	-0.157	-0.349
N10	-0.113	-0.42	-0.216	-0.52	-0.276	-0.537	-0.259	-0.52
H11	0.381	0.472	0.373	0.471	0.403	0.465	0.392	0.469
	G3 Protonation at N3		**G3 Protonation at N6**		**G3 Protonation at N9**		**G3 Protonation at N10**	
	Mulliken	NBO	Mulliken	NBO	Mulliken	NBO	Mulliken	NBO
C1	0.141	0.46	0.223	0.372	0.301	0.464	0.342	0.454
C2	0.56	0.75	0.28	0.574	0.481	0.785	0.488	0.72
N3	0.194	-0.443	-0.181	-0.381	-0.178	-0.387	-0.16	-0.34
H4	0.246	0.47	0.282	0.452	0.304	0.476	0.312	0.464
H5	0.267	0.245	0.249	0.226	0.26	0.235	0.284	0.262
N6	-0.459	-0.805	0.129	-0.687	-0.401	-0.82	-0.383	-0.837
H7	0.271	0.435	0.247	0.468	0.25	0.428	0.26	0.417
H8	0.267	0.433	0.247	0.468	0.262	0.427	0.236	0.416
N9	-0.374	-0.493	-0.227	-0.348	-0.028	-0.422	-0.303	-0.417
N10	-0.359	-0.52	-0.52	-0.617	-0.569	-0.659	-0.358	-0.608
H11	0.246	0.47	0.269	0.471	0.316	0.473	0.284	0.477

It would be interesting to investigate the molecular properties of the protonated ATA species and compare these properties with those of the neutral ATA species to determine the preferred species that bind themselves to a metal surface. The preferred site for protonation is determined by comparing the proton affinity (PA) at different sites. For all active sites, the PA of the inhibitor was calculated using the following equation:

$$PA = E_{prot} + E_{H_2O} - E_{non-prot} - E_{H_3O^+}$$

Where E_{prot} and $E_{non-prot}$ are the total energies of the protonated and the non-protonated forms of the ATA inhibitor respectively, E_{H_2O} is the total energy of a water molecule and $E_{H_3O^+}$ is the total energy of the hydronium ion. A high value of PA indicates that the molecule has a high tendency to be protonated. The calculated PA values for the protonated ATA species are shown in Table 7. The protonated species have lowest PA in the gas phase. The data obtained by B3LYP and G3 methods indicate that for both phases the preferred site for protonation is the N10 atom.

Table 7: PA values for the protonated species: [a] MP2 and [b] G3

	Gas	**Solvent**
B3LYP Protonation at N3	-0.811	0.063
B3LYP Protonation at N6	-1.715	-0.946
B3LYP Protonation at N9	-2.151	-1.176
B3LYP Protonation at N10	-2.341	-1.352
G3 Protonation at N3	-0.573[a] -0.832[b]	0.309[a] 0.049[b]
G3 Protonation at N6	-1.783[a] -1.717[b]	-0.977[a] -0.913[b]
G3 Protonation at N9	-1.899[a] -2.064[b]	-0.960[a] -1.129
G3 Protonation at N10	-2.228[a] -2.288[b]	-1.228[a] -1.301[b]

In order to make a meaningful comparison between the protonated and non-protonated structures of the ATA molecule, only protonations on the nitrogen atoms need to be investigated. A comparison between Tables 1 and 4 shows that the charge (*e*) on the N3 atom is higher for both phases in the N3-protonated form than in the non-protonated form and the charges on the N3, N6, N9 and N10 atoms is higher for both phases in the non-protonated form than in their protonated forms. These results show that the charges on the nitrogen atoms are almost reduced in the protonated forms. For example, the charges, calculated by the B3LYP method, for the N3, N6, N9, N10 atoms of the N6-protonated ATA decrease by 0.045, 0.125, 0.107 and 0.061 respectively, and the charges for the same atoms, calculated by the G3 method, decrease by 0.093, 036, 0.154, 0.129 and 0.065, respectively. The Mulliken charges and NBO data obtained using B3LYP/6-311++G (d, p) are significantly different from the G3 method data. These data are consistent with the fact that Mulliken charges and NBO data are strongly method sensitive. A comparison between the quantum chemical parameters of the protonated ATA species (Table 4) and those of the non-protonated ATA species (Table 1) show similarity of the two forms. For instance, both B3LYP and G3 methods produce a low ΔE for the non-protonated form in the gas phase, but in the case of the protonated form, the B3LYP method gives a low ΔE value in the liquid phase whereas the G3 method gives a low ΔE value in the gas phase.

A comparison between the individual values of E_{HOMO}, E_{LUMO} and ΔE, calculated by the B3LYP and G3 methods, shows that for the two phases E_{HOMO} of the protonated form is lower than E_{HOMO} of the non-protonated form. It means that the non-protonated form has a greater tendency to donate an electron pair than the protonated form. E_{LUMO} values of the protonated forms, calculated by both B3LYP and G3 methods, are for both phases lower than those of the non-protonated form suggesting that the protonated forms have a greater tendency to accept electrons than the non-protonated species. The G3 method computes a smaller ΔE for the non-protonated form than for the protonated form, indicatinging that in the two phases the non-protonated form has a greater reactivity than the protonated form. The B3LYP method calculates a smaller ΔE for the N3 and N10 protonated forms than for the non-protonated form, meaning that the N3 and N10 protonated forms have a greater tendency to be adsorbed on a metal surface than the non-protonated form in both phases.

The G3 method works out a smaller global softness for the non-protonated form than in the protonated form, meaning that in the two phases the non-protonated form has a greater reactivity than the protonated form. But the B3LYP method gives a smaller ΔE for the N3 and N10 protonated forms than for their corresponding non-protonated form, meaning that the protonated form has a greater tendency to be adsorbed on a metal surface than the non-protonated form in the two phases.

Table 3 shows that the G3 method gives for the two phases the highest σ values for the non-protonated form which indicates the high reactivity of this form. The B3LYP method gives the highest σ values for N3 and N10 protonated forms in the two phases, which indicates the high reactivity of these forms.

The two methods calculate a higher dipole moment for the protonated ATA species than for its non-protonated conjugate, which suggests that dipole-dipole interactions are more predominant in the interaction between the metal surface and the protonated forms than in the interaction between the metal surface and the non-protonated form. Both methods appear to give for both phases a higher sum of the negative charges for the non-protonated form than for the protonated forms.

The following conclusions may be drawn from the results of the molecular properties of the protonated ATA species:

(1) The quantum chemical descriptors of the protonated species obtained by the B3LYP method in the gas phase and in solution are different from those obtained by the G3 method.

(2) A comparison between the molecular properties of the studied compounds in the gas phase and in aqueous solution provides information about the solvent effects on the molecular properties.

(3) The N6 atom has the highest negative charge in the two phases.

Conclusion

The quantum chemical descriptors of the ATA inhibitor were calculated using the density functional theory at the B3LYP/6-311G++ (d, p) basis set. The G3 method was used in order to obtain more reliable energies of all stationary points on the PES. Because the quantum chemical descriptors are strongly dependent on energy, the PES calculation method is very important. For this reason, the results of the quantum chemical descriptors of the species which were calculated by the B3LYP method are different from those obtained using the G3 method in the gas phase and in solution. This work has shown that the effect of solvent on corrosion inhibition is important and the protonated ATA species are less adsorbed on a metal surface than the neutral species. The results of the molecular properties of the protonated ATA species compared with those of the neutral ATA species shows: a) the neutral species have a greater tendency to donate electrons and therefore bind stronger to metal surfaces both in the gas phase and in solution. b) The ΔE values suggest that the neutral species are more reactive than the protonated species in both phases. c) The corrosion inhibition effectiveness of neutral species is higher than that of protonated species and this property is more evident by the G3 method data than those of the B3LYP method. d) It is reasonable to infer that the protonated species are less likely to interact with metal surfaces. e) Physisorption and chemisorption mechanisms are involved in the adsorption process of ATA on steel surfaces. f) The N6 atom has the highest negative charge both in the protonated and in the neutral species and that for both gas phase and solution states.

Acknowledgements

This work was supported by Graduate University of Advanced Technology and Research Center for Science, High Technology & Environmental Science, Kerman. This article was peer reviewed by Nasser Mirzai Baghini, Imperial College Reactor Centre, Silwood Park, Ascot, Berkshire, United Kingdom.

References

[1] Zhang, G.; Musgrave, C. B., *J. Phy. Chem. A.*, 2007, 111, 1554.
[2] Bereket, G.; Hur, E.; Ogretir, C., *J. Mol. Struct.*, 2002, 578, 79.
[3] Kabanda, M. M.; Ebenso, E. E., *Int. J. Electrochem. Sci.*, 2012, 7, 8713.
[4] Parr, R. G.; Yang, W., Density Functional Theory of Atoms and Molecules, Oxford University Press: New York, 1989.
[5] Ebenso, E. E.; Kabanda, M. M.; Murulana, L. C.; Singh, A. K.; Shukla, S. K., *Ind. Eng. Chem. Res.*, 2012, 51, 12940.
[6] Kabanda, M. M.; Murulana, L.C.; Ozcan, M.; Karadag, F.; Dehri, I.; Obot, I.B.; Ebenso, E.E., *Int. J. Electrochem. Sci.*, 2012, 7, 5035.
[7] Ebenso, E.E.; Arslan, T.; Kandemirli, F.; Caner, N.; Love. I., *Int. J. Quant. Chem.*, 2010, 110, 1003.
[8] Senet, P., *Chem. Phys. Lett.*, 1997, 275, 527.
[9] Solmaz, R.; Kardaş, G.; Culha, M.; Yazici B.; Erbil M., *Electrochim. Acta.*, 2008, 53, 5941.
[10] Kosari, A.; Momeni, M.; Parvizi, R.; Zakeri, M.; Moayed, M. H.; Davoodi, A.; Eshghi, H., *Corros. Sci.*, 2008, 53, 3058.
[11] Khaled, K. F.; Fadl-Allah, S. A.; Hammouti, B., *Mater. Chem. Phys.*, 2009, 117, 148.
[12] Wang, L., *Corros. Sci.*, 2006, 48, 608.
[13] Bastidas, J. M.; Otero, E., *Mater. Corros.*, 1996, 47, 333.
[14] Tang, Y.; Yang, X.; Yang, W.; Wan, R.; Chen, Y.; Yin, X., *Corros. Sci.*, 2010, 52, 1801.
[15] Khaled, K. F., *Electrochim. Acta.*, 2008, 53, 3484.
[16] Musa, A.Y.; Kadhum, A. A. H.; Mohamad, A. B.; Takriff, M. S., *Corros. Sci.*, 2010, 52, 3331.
[17] Zheludkevich, M.L.; Yasakau, K. A.; Poznyak, S. K.; Ferreira, M. G. S., *Corros. Sci.*, 2005, 47, 3368.
[18] Kokalj, A.; Peljhan, S., *Langmuir.*, 2010, 26(18), 14582.
[19] Awad, M. K.; Mustafa, M. R., *J. Mol. Struct.*, 2010, 959, 66.
[20] Ibrahim, M. A. M.; Abd El Rehim, S. S.; Hamza, M. M., *Sci. Int. J.*, 2014, 4, 940.
[21] Doner, A.; Solmaz, R.; Ozcan, M.; Kardas, G., *Corros. Sci.*, 2011, 53, 2902.
[22] Frisch, M. J.; Truck, G. W.; Schlegel, H. B.; Scuseria, G. E.; Robb, M. A.; Cheeseman, J. R.; Zakrzewski, V. G.; Montgomery, J. A.; Jr.; Stratmann, R. E.; Burant, J. C.; Dapprich, S.; Millam, J. M.; Daniels, A. D.; Kudin, K. N.; Strain, M. C.; Farkas, O.; Tomasi, J.; Barone, V.;Cossi, M.; Cammi, R.; Mennucci, B.; Pomelli, C.; Adamo, C.; Clifford, S.; Ochterski, J.; Petersson, G. A.; Ayala, P. Y.; Cui, Q.; Morokuma, K.; Malick, D. K.; Rabuck, A. D.; Raghavachari, K.; Foresman, J. B.; Cioslowski, J.; Ortiz, J. V.; Boboul, A. G.; Stefnov, B.B.; Liu, G.; Liaschenko, A.; Piskorz, P.; Komaromi, L.; Gomperts, R.; Martin, R. L.; Fox, D. J.; Keith, T.; Al-Laham, M. A.; Peng, C. Y.; Nanayakkara, A.; Gonzalez, C.; Challacombe, M.; Gill, P. M. W.; Johnson, B.; Chen, W.; Wong, M. W.; Andres, J. L.; Gonzalez, C.; HeaGordon, M.; Replogle E. S.; Pople, J. A., 2003, GAUSSIAN 03, Revision A.1, Guassian, Inc., Pittsburgh, PA.
[23] Curtiss, L. A.; Raghavachari, K.; Redfern, P. C.; Rassolov, V.; Pople, J. A., *J. Chem. Phys.*, 1998. 109, 7764.
[24] Cancès, E.; Mennucic, B.; Tomasi, J., *J. Chem. Phys.*, 1997, 107, 3032.
[25] Chipman, D. M., *J. Chem. Phys.*, 2000, 112, 5558.
[26] Tomasi, J.; Mennucci, B.; Cancès, E., *J. Mol. Struct.*, 1999, 464, 211.
[27] Lashkari, M.; Arshadi, M. R., *Chem. Phys.*, 2004, 299, 131.
[28] Cances, E.; Mennucci, B.; Tomasi, J., *J. Chem. Phys.*, 1997, 107, 3032.
[29] Chandra, A. K.; Nguyen, M. T., *Int. J. Mol. Sci.*, 2002, 3, 310.
[30] Stayanov, R. S.; Gusarov, S.; Kovalenko, A., *Molecular Simulation*, 2008, 34, 943.
[31] Gece, G.; Bilgic, S., *Corros. Sci.*, 2009, 51, 1876.
[32] Ahamad, I.; Prasad, R.; Quraishi, M. A., *Corros. Sci.*, 2010, 52, 1472.
[33] Rajak, K. S.; Islam, N.; Ghosh, D. C., *J. Quantum. Info. Science*, 2011, 1, 87.

[34] Obi-Egbedi, N.O.; Obot, I.B.; El-Khaiary, M. I.; Umoren, S.A.; Ebenso, E. E., *Int. J. Electro. Chem. Sci.*, 2011, 6, 5649.
[35] Parr, R.G.; Szentpaly, L.; Liu, S., *J. Am. Chem. Soc.*, 1999, 121, 1922.
[36] Gázquez, J. L.; Cedillo, A.; Vela, A. *J. Phy. Chem. A*, 2007, 111, 1966.
[37] Khaled, K. F., *Electrochim. Acta*, 2010, 55, 6523.
[38] Lukovits, I.; Kalman, E.; Zucchi, F., *Corros.*, 2001, 57, 3.
[39] Sastri, V. S.; Perumareddi, J. R., *Corrosi.*, 1997, 53, 617.
[40] Li, X.; Deng, S.; Fu, H.; Li, T., *Electrochim. Acta*, 2009, 54, 4089.
[41] Gece, G.; Bilgic, S., *Corros. Sci.*, 2010, 52, 3435.
[42] Yang, Y.; Mortier, W. J., *J. Am. Chem. Soc.*, 1986,108, 5708.